Synaptic plasticity and learning behaviours in flexible artificial synapse based on polymer/viologen system†

Chaochao Zhang,‡[abc] Yu-Tsung Tai,‡[d] Jie Shang,‡[ab] Gang Liu,*[ab] Kun-Li Wang,*[d] Chienwen Hsu,[d] Xiaohui Yi,[ab] Xi Yang,[ab] Wuhong Xue,[ab] Hongwei Tan,[ab] Shanshan Guo,[ab] Liang Pan[ab] and Run-Wei Li*[ab]

In this study, an artificial synapse with a sandwich structure of Ta/ethyl viologen diperchlorate [EV(ClO_4)$_2$]/triphenylamine-based polyimide (TPA-PI)/Pt is fabricated directly on a flexible PET substrate and exhibits distinctive history-dependent memristive behaviour, which meets the basic requirements for synapse emulation. Essential synaptic plasticity (including long-term plasticity and short-term plasticity) and some memory and learning behaviours of human beings (including the conversion from short-term memory to long-term memory and the "learning–forgetting–relearning") have been demonstrated in our device. More importantly, the device still exhibits the synaptic performance when the surface strain of the device reaches 0.64% (or, the bending radius reaches 10 mm). Moreover, the device was able to endure 100 bending cycles. Our findings strongly demonstrate that the organic artificial synapse is not only promising for constructing a neuromorphic information storage and processing system, but is also interesting for the realization of wearable neuromorphic computing systems.

Introduction

All kinds of complex life activities are controlled by the brain, including learning, memory, perception and emotion, which have attracted a considerable amount of attention in order to investigate the most powerful information processors like the brain.[1,2] The circuitry of the human brain is composed of a trillion (10^{12}) neurons, and each neuron connects with others by up to 1000 synapses.[3] The synapse is believed to underlie learning and memory due to synaptic plasticity, where synaptic weight, namely the connection strength between neurons, can be continuously modulated by synaptic inputs.[4–7] Therefore, synapse emulation is considered as a preliminary step towards a highly effective artificial brain neural network.[8–12] Previously, a complementary metal-oxide–semiconductor (CMOS) combined with multiple transistors and capacitors is used to imitate a single synapse, which would increase the energy consumption and complexity of integrated circuits (ICs),[13–17] leading to it being hard to obtain high-density neural networks. Therefore, it is necessary to develop a novel component to simulate the function of a single synapse. The memristor is considered to be such a component.[18–20] Its resistance can be changed continuously that is very similar to the continuous modulation characteristics of synaptic weight.[21] At present, some memristors have triumphantly realized the function simulation of synapses, including potentiation and depression of synaptic weight, long-term/short-term plasticity (LTP/STP) and non-associative/associative memory,[22–28] and so on. However, most of the reported materials for simulating biological synapses are inorganic materials which are fragile[22–28] and will not likely work well for flexible electronics, especially for wearable devices. Compared with inorganic materials, organic materials bear advantages of large-area processability, mechanical flexibility, light-weight and low-cost applications.[29–31]

Recently, some research groups also successfully fabricated artificial synapses using organic materials such as PEDOT:PSS,[22,32] PFD-8CN,[33] EV(ClO_4)$_2$/BTPA-F[34] and chitosan.[35] But the organic materials above are still mainly grown on rigid substrates,[22,32–34] so the influence of flexural deformation on synaptic performance has not been paid enough attention,

[a] Key Laboratory of Magnetic Materials and Devices, Ningbo Institute of Materials Technology and Engineering, Chinese Academy of Sciences, Ningbo 315201, P. R. China. E-mail: liug@nimte.ac.cn, runweili@nimte.ac.cn; Fax: +86-574-8632-4675; Tel: +86-574-8632-4675
[b] Zhejiang Province Key Laboratory of Magnetic Materials and Application Technology, Ningbo Institute of Materials Technology and Engineering, Chinese Academy of Sciences, Ningbo 315201, P. R. China
[c] Department of Chemistry, Shanghai University, Shanghai 200444, P. R. China
[d] Department of Chemical Engineering and Biotechnology, National Taipei University of Technology, Taipei 10608, Taiwan. E-mail: klwang@ntut.edu.tw

although it is important for practical flexible application to measure synaptic performance in the bent state.[36]

In this study, the polyimide based on triphenylamine (TPA-PI) has been synthesized *via* condensation polymerization. An artificial synapse with a sandwich structure of Ta/EV(ClO_4)$_2$ (ethyl viologen diperchlorate)/TPA-PI/Pt is fabricated directly on a flexible PET substrate. TPA-PI can be reversibly changed between insulating and conducting states since triphenylamine units can exhibit rich electrochemical redox behaviour.[37,38] In addition, EV(ClO_4)$_2$ is a good choice for the counter-reaction of TPA-PI oxidation because it exhibits electrochemically reversible redox properties.[39,40] Perchlorate (ClO^{4-}) acts as a counter ion to synchronously stabilize the charged form of the oxidized TPA-PI.[39–41] In order to improve the migration rate of ClO^{4-}, a polyethylene oxide (PEO) matrix also has been used as a solid electrolyte.[39,40,42] Using this single artificial synapse, we have successfully emulated essential synaptic plasticity (including long-term plasticity and short-term plasticity) and some memory and learning behaviours of human beings (including the conversion from short-term memory to long-term memory and the ''learning–forgetting–relearning'') process. What is more, we have also studied the synaptic performance it the bent state and the influence of bending radius and bending times on synaptic simulation. These findings show the possibility of utilizing organic materials for the realization of wearable neuromorphic computing systems.

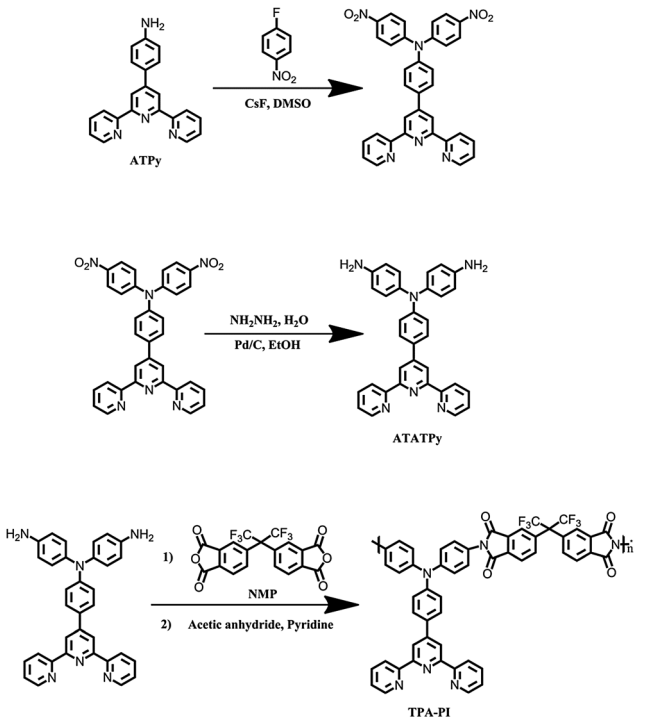

Scheme 1 Synthetic routes of the ATATPy and TPA-PI.

Experimental section

Material synthesis and characterization

N-(4-Aminophenyl)-*N*-(4-(2,6-di(pyridin-2-yl)pyridine-4-yl) phenyl)-benzene-1,4-diamine (ATATPy) was synthesized according to Scheme 1. TPA-PI was synthesized *via* condensation polymerization of ATATPy with 4,4′-(hexafluoro-isopropylidine)bisphthalic anhydride (6FDA). More specifically, in a 25 mL three-neck round-bottom flask equipped with a stirring bar, 0.7532 g (1.488 mmol) of ATATPy and an equal molar ratio of 6FDA were dissolved in 7 mL of anhydrous *N*-methyl-2-pyrrolidone (NMP) under a nitrogen atmosphere. After 4 h of stirring at room temperature, 3.2 mL of acetic anhydride and 1.6 mL of pyridine were added to the mixture, after which, the suspension solution was heated for 4 h. Afterwards, the crude polymeric product was precipitated by adding deionized water. The crude product was then collected by filtration and dried *in vacuo* at 80 °C. Then, the obtained product was subjected to Soxhlet extraction with hot methanol to remove the unreacted monomers and dried *in vacuo* at 80 °C. FT-IR (KBr, cm^{-1}) (Fig. S1, ESI†): 1785, 1722 (C═O). ^{1}H-NMR ($CDCl_3$, ppm) (Fig. S2, ESI†): δ 8.72–8.76 (br, 6H, ArH), δ 7.89–8.05 (br, 10H, ArH), δ 7.36–7.39 (br, 12H, ArH). M_n = 1.30 × 10^5, M_w = 1.45 × 10^5. Normally, aromatic polyimides are characterized as highly thermally stable polymers.[43,44] As predicted, thermogravimetric analysis (TGA) suggests that TPA-PI exhibits excellent thermal stability, with no significant weight loss below 538 °C in air and nitrogen atmosphere (Fig. S3, ESI†). Meanwhile, TPA-PI can exhibit electrochemical redox behaviour (Fig. S4, ESI†). Other chemicals were purchased from Sigma-Aldrich (Shanghai, China) and utilized directly without further purification.

Device fabrication

The PET substrate was pre-cleaned in acetone, ethanol and deionized water in an ultrasonic bath, in that order and each for 20 minutes, followed by drying in a nitrogen flow. A Pt electrode of 50 nm thickness was deposited on the PET substrate by DC reactive magnetron sputtering at room temperature under vacuum (10^{-5} Pa). The TPA-PI solution of 5 mg mL^{-1} was prepared *via* dissolving the polymer powders in cyclohexanone. The pre-prepared solution was filtered by using a micro-filter with polytetrafluoroethylene (PTFE) membrane with a pore size of 0.45 μm to remove any undissolved particles. The TPA-PI functional layer was then deposited by spin-coating 50 μL solution of the polymer on the Pt/PET substrate at a rotational speed of 500 rpm for 10 s and then at 1000 rpm for 60 s, followed by drying and annealing in a vacuum oven at 70 °C for 2 h. The electrolyte solution (EV(ClO_4)$_2$ and PEO dissolved in acetonitrile) was prepared according to the existing method.[39] The method of fabricating the electrolyte layer is similar to the TPA-PI functional layer. A circular Ta electrode with a radius of 500 μm and thickness of 60 nm was deposited on the electrolyte layer by direct current (DC) reactive magnetron sputtering through a shadow mask.

Measurements

The current–voltage (*I*–*V*) characteristics of the Ta/EV(ClO_4)$_2$/TPA-PI/Pt device were measured with a Keithley 4200 semiconductor

parameter analyser under ambient atmosphere, and the Pt electrode was grounded during electrical measurements. In addition, the device was bent with a home-modified vernier caliper with digital display (the bending radii were previously converted to the direct distances between the two measurement claws of the vernier caliper).

The ^{1}H nuclear magnetic resonance (^{1}H NMR) spectrum was measured at 400 MHz on a Bruker 400 AVANCE III spectrometer with chloroform ($CDCl_3$) as solvent and tetramethylsilane (TMS) as reference for the chemical shifts. The Fourier transform infrared (FT-IR) spectrum was recorded on a Thermo Nicolet 6700 FTIR spectrophotometer through dispersing the powder of polymer in a KBr pellet. Number-average (M_n) and weight-average (M_w) molecular weights were measured by gel permeation chromatography (GPC) using linear polystyrene as the molecular weight standards and *N*-methyl-2-pyrrolidone (NMP, 1 mL min^{-1}) as the eluent. Thermogravimetric analysis (TGA) was monitored on a Perkin-Elmer Diamond TG/DTA instrument in a nitrogen atmosphere or an ambient atmosphere with the heating rate of 20 °C min^{-1} from 30 °C to 800 °C and a gas-flow rate of 50 mL min^{-1}. Cyclic voltammetry (CV) measurements were recorded in a 0.1 M electrolyte solution of tetrabutylammonium perchlorate (n-Bu_4NClO_4) dissolved in acetonitrile under an argon atmosphere with a scan rate of 50 mV s^{-1}, using the polymer film coated on Pt electrode as the working electrode, platinum gauze and Ag/AgCl (3.8 M KCl) as the counter and reference electrodes, respectively. The cross-sectional image of the $EV(ClO_4)_2$/TPA-PI bilayer structure was obtained from a Hitachi S-4800 field-emission scanning electron microscope.

Results and discussion

Basic electrical characteristics

Using the above mentioned organic redox system, we prepared an artificial synapse device based on Ta/320 nm $EV(ClO_4)_2$/230 nm TPA-PI/Pt sandwich structure (Fig. 1(a) and Fig. S5, ESI†). The Ta/$EV(ClO_4)_2$/TPA-PI/Pt device exhibits a distinctive history-dependent memristive behaviour at room temperature, as plotted in the current–voltage (*I*–*V*) characteristics of Fig. 1(b). Upon being subjected to four cumulative positive voltage sweeps of 0 V → 0.5 V → 0 V, the device conductance can be increased consecutively, which demonstrates a synaptic potentiation characteristic. The potentiation characteristic is caused by electrochemical oxidation of TPA-PI. Upon electrochemical oxidation of the polymer, a radical cation is formed that markedly increases the conductance of the TPA-PI polymer and the device.[22,34,39] Afterwards, five cumulative negative voltage sweeps of 0 V → −0.5 V → 0 V were applied to the device, while the device conductance can be decreased continuously, which demonstrates a synaptic depression characteristic. The depression characteristic is due to the reduction of the TPA-PI radical cation, which switches the device back to the initial low conductive state.[22,34,39] In order to clearly illustrate such a changing trend, the curve of sweeping voltage and responding current *versus* time was plotted (Fig. 1(c)). Compared with the previous works,[20,22,25,26] the device exhibits a low operational voltage (∼±0.5 V) that can effectively reduce the power consumption. Besides that, a slight rectifying effect is observed. This phenomenon may be attributed to the difference in the work functions of the top/bottom electrode materials and the molecular orbital energy levels of the TPA-PI polymer and the $EV(ClO_4)_2$, which influences the charge transport across the $EV(ClO_4)_2$/TPA-PI junction under electric fields of different polarity.[34] Also, such a rectifying effect contributes to the single-direction transmission of a signal in biological synapses.[45,46] Besides that, the potentiation and depression of synaptic weight (the current can be regarded as the synaptic weight) are also observed when 90 consecutive positive voltage pulses with an amplitude of 0.5 V and a duration of 10 ms, and immediately 90 following consecutive negative voltage pulses with an amplitude of −0.5 V and a duration of 10 ms are applied onto the device (Fig. 1(d)). The reliability and reversibility of synaptic potentiation/depression characteristics are also evaluated in Fig. S6 (ESI†).

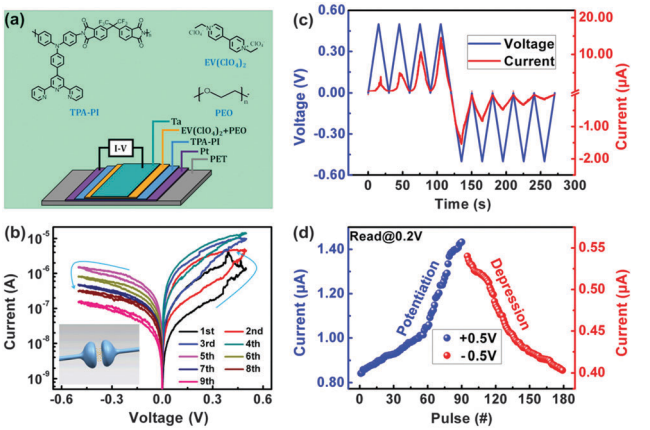

Fig. 1 (a) Chemical structures of TPA-PI, $EV(ClO_4)_2$ and PEO, as well as the schematic illustration of the artificial synapse device. (b) The current–voltage characteristics of the Ta/$EV(ClO_4)_2$/TPA-PI/Pt device showing distinctive history-dependent memristive behaviour. Inset: Diagram of a biological synapse. (c) Applied voltage and measured current plotted against time, illustrating the variation trend in current during consecutive voltage sweeps. (d) Currents obtained after a series of 90 positive pulses (0.5 V, 10 ms) followed by 90 negative pulses (−0.5 V, 10 ms) applied to the device. The data points are monitored at ±0.2 V.

Synaptic plasticity

In neuromorphic systems, the ability to continuously adjust the synaptic weight, *i.e.* the potentiation and depression of synapses, is called synaptic plasticity, which is considered as the basic characteristic of human brain learning and memory functions.[47,48] In the case of synaptic plasticity, it can be categorized into short-term plasticity (STP) and long-term plasticity (LTP).[49–51] In neuroscience, it is generally thought that STP influences the learning and memory behaviour of the human brain. The nervous system endlessly receives huge amounts of information from the outside world, so it is vital to extract useful information from the gigantic quantity of external information. In neural systems, the STP of a

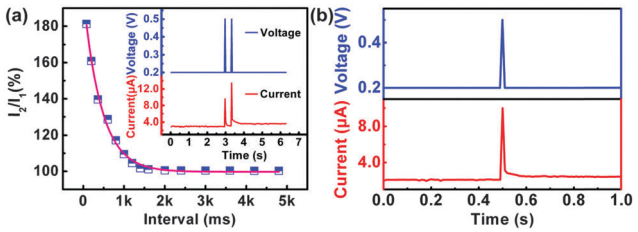

Fig. 2 (a) The ratio of response currents (I_2/I_1) *versus* time interval between two spikes. The solid line is the exponential fit to the experimental data. Inset: The paired-pulse facilitation (PPF) measured with two successive spikes (0.5 V, 10 ms). (b) The excitatory postsynaptic current (EPSC) evoked with a pulse stimulation (0.5 V, 10 ms).

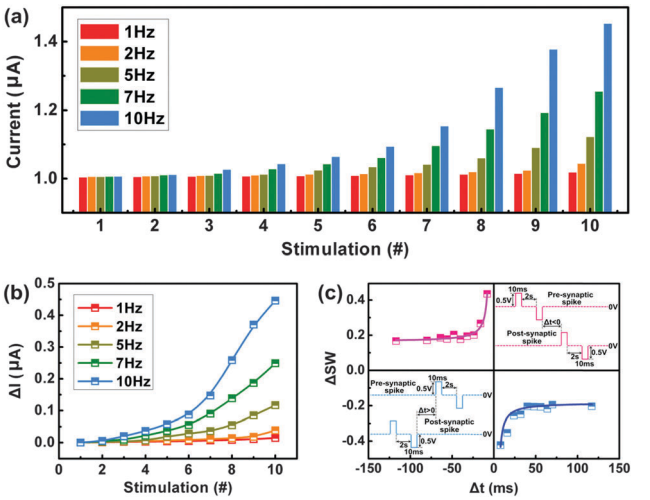

Fig. 3 (a) Variation in current with the stimulation number for different spike rates. The current is recorded with a small read voltage (0.2 V) immediately after each stimulation (0.5 V, 10 ms). (b) The change of current increase *versus* number of stimulation for different spike rates. (c) The variation of synaptic weight (ΔSW) *versus* relative spike timing (Δ*t*) of the presynaptic and postsynaptic paired-spike implementation. The data points are fitted with exponential functions.

biological synapse is deemed to play a key role in information extraction.[50,52] As a common form of STP in biological synapses, paired-pulse facilitation (PPF) reflects that the second postsynaptic response motivated by the pulse is larger than the first one.[53–55] Such a PPF behaviour can be mimicked in our artificial synapse device. As shown in the inset of Fig. 2(a), when the device receives two continuous voltage stimuli (0.5 V, 10 ms), the current response (I_2) triggered by the second pulse is larger than the first one (I_1). In addition, it can be seen from Fig. 2(a) that the ratio (I_2/I_1) is determined by the time interval between the two pulses, which can be attributed to the excitatory postsynaptic current (EPSC).[7,20,56] From the inset of Fig. 2(a), we can find the current response gradually decays to a steady value after pulsed bias, which is similar to the behaviour of EPSC in a biological excitatory synapse. In order to more clearly illustrate the EPSC, a single spike (0.5 V, 10 ms) is applied to trigger an EPSC, which may be ascribed to the inertia effect of the ionic flux.[20,34] We could see that its intensity gradually decays to a steady value within about 60 ms after the spike (Fig. 2(b)). The life time of the evoked EPSC is longer than that of the applied pulse, and so contributes to the current overlap when the time interval between the paired pulses is relatively short. Furthermore, a larger overlap of the evoked EPSC would be provoked by a shorter time interval.

In addition to STP, there is another synaptic plasticity LTP which also plays an important role in the synaptic mechanism of learning and memory storage, as LTP means a persistent change to the synaptic weight.[57,58] Meanwhile, LTP is influenced by spike rate and spike timing.[7,59–63] Herein, we first investigate the impact of spike rates from 1 Hz to 10 Hz on LTP, as shown in Fig. 3(a) and (b). From Fig. 3(a), we can see that the more frequent stimuli lead to larger increases of the current. At the spiking rate of 1 Hz, the current exhibits no significant increase with the increasing pulse numbers. When the spiking rate reaches 10 Hz, the current is increased from 1 μA to 1.45 μA. This indicates that the present device can also act as a high-pass filter. In order to more clearly analyze the current increases, the relative change of current ($\Delta I = I_N - I_1$, where I_N and I_1 are the corresponding current after the *N*th and 1st pulse, respectively) *versus* the pulse number is re-plotted in Fig. 3(b). In addition to spike rate, the impact of spike timing on LTP is also explored. Spike timing means the temporal order of the pre- and postsynaptic spikes. Specifically, the polarity of the synaptic weight change depends on the spike timing. When the postsynaptic spike is stimulated instantly after the presynaptic spike (*i.e.* $\Delta t = t_{pre} - t_{post} < 0$, Δt is the time interval from the end of the presynaptic spike to the beginning of the postsynaptic spike), the synaptic weight is potentiated. Instead, the synaptic weight gets depressed (Fig. 3(c)). Simultaneously, both depression and potentiation of synaptic weight are adjustable with the time interval. A smaller time interval can result in a heavier variation of synaptic weight ($\Delta SW = (I_2 - I_1)/I_1$, where I_1 and I_2 are the postsynaptic currents measured before and 10 minutes after the paired-spike application, respectively).

Memory and learning behaviours

In the study of neurobiology, STP and LTP correspond to the short-term memory (STM) and long-term memory (LTM), respectively, and the memory is considered to be closely related with the strength of synaptic connection or synaptic weight.[47,64] For the human memory model, STM decays rapidly with time, so it can only be transient maintained by applying stimulation.[65–67] In contrast, LTM can be sustained for a relatively longer time without any followed stimulus because of lasting changes in certain synaptic structures.[68,69] Therefore, understanding of the STM and LTM will be beneficial for improving the memory capability.[70,71] Below we show the conversion from STM to LTM by constantly rehearsing the same stimuli.[10,72] As illustrated in Fig. 4(a), six pulse voltages (amplitude = 0.5 V, duration = 10 ms, period = 800 ms) and a constant 0.2 V pedestal voltage are applied to the present $EV(ClO_4)_2$/TPA-PI bilayer (blue curve in Fig. 4(a)). The competition effect between spontaneous current weakening after each pulse and overall current strengthening upon the constant pulses is similar to the competition effect of memory loss and memory enhancement in

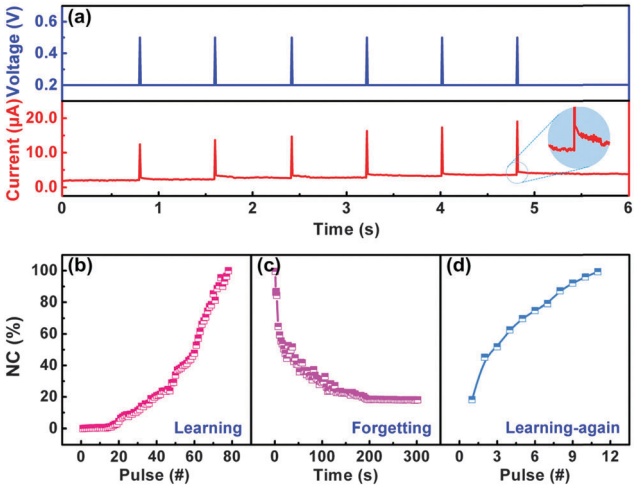

Fig. 4 (a) The corresponding current *versus* the voltage applied to the device, consisting of six 0.5 V, 10 ms pulses and a constant 0.2 V pedestal voltage. (b–d) Demonstration of the "learning–forgetting–relearning" process. The learning process is performed with 80 consecutive stimuli (0.5 V, 10 ms). The forgetting process is then recorded without stimuli and the solid line is the exponential fit to the experimental data. The relearning process is conducted with 11 consecutive stimuli (0.5 V, 10 ms). The data points are all monitored at 0.2 V.

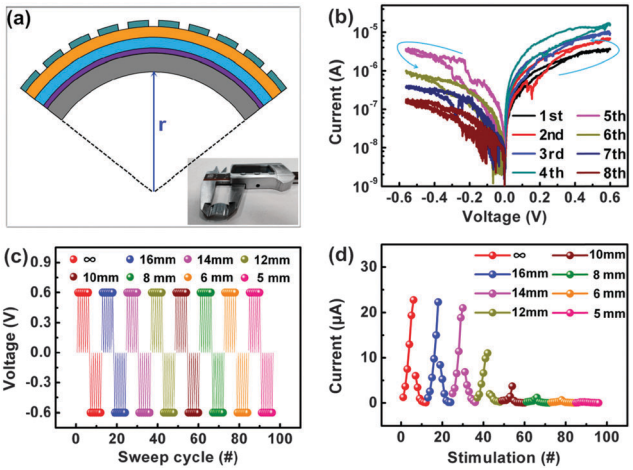

Fig. 5 (a) Schematic illustration of the flexible artificial synapse bent at a certain convex radius. Inset: The digital image of the bending sample along the long-axis direction with a vernier caliper. (b) *I*–*V* characteristics of the device at continuous positive (negative) scanning voltage 0.5 V (−0.5 V) when the device was bent at r = 16 mm. (c) Profile of the positive (negative) scanning voltages of ±0.5 V applied at different curvature radii. (d) Variation of the synaptic potentiation and synaptic depression characteristics at different curvature radii.

biological systems (red curve in Fig. 4(a)). Another interesting human-learning behaviour can also be observed in the device (Fig. 4(b)–(d)). When 80 continuous stimuli (0.5 V, 10 ms) are applied to the device, the normalized current (NC) gradually increases with the number of pulses (Fig. 4(b)). When the applied stimuli are removed, the NC spontaneously decays which may be ascribed to the spontaneous diffusion of the TPA-PI radical cation through inter-chain hopping.[20,39] The decay trend is slow after the initial fast dropping stage, which is consistent with the forgetting curve of Ebbinghaus in psychology (Fig. 4(c)).[73,74] Simultaneously, the NC does not decay to the initial value, but stabilizes at an intermediate value, which demonstrates the existence of LTM in the process of forgetting. When the device is stimulated again with the same stimulus, fewer stimuli are adequate to recover the memory level (Fig. 4(d)). This behaviour is similar to the learning-again (or recalling) process of human beings, that forgotten information can be learned again faster.

Bending measurement

To study the synaptic performance of the device in the bent state, the Ta/EV$(ClO_4)_2$/TPA-PI/Pt structure was grown on a flexible PET substrate (15 mm × 10 mm). The device was bent along the long-axis direction with a vernier caliper, as shown in Fig. 5(a). The surface strain at different curvature radii (r) was estimated (Fig. S7, ESI†). Herein, the synaptic potentiation, synaptic depression and EPSC are studied in the bent state, which is the basis to realize the above synaptic functions and memory behaviours. In Fig. 5(b), the device current can be increased and decreased continuously with the cumulative positive voltage sweeps (0.5 V, 30 mV s^{-1}) and negative voltage sweeps (−0.5 V, 30 mV s^{-1}) when the bending radius is equal to 16 mm (*i.e.* r = 16 mm). This behaviour is similar to the synaptic potentiation and synaptic depression characteristics in the flat state (Fig. 1(b)), which demonstrates the stability of the device. Besides, the EPSC can be evoked by a single pulse (0.5 V, 10 ms) at r = 16 mm (Fig. S8, ESI†). Next, we also study the impact of bending radii (flat, r = 16 mm, 14 mm, 12 mm, 10 mm, 8 mm, 6 mm, 5 mm, respectively) at a 0.5 V scanning voltage (Fig. 5(c)). When the device is bent from the flat state to r = 14 mm, the synaptic potentiation and synaptic depression characteristics exhibit no obvious change (Fig. 5(d)). At the bending radius of 10 mm, the potentiation/depression characteristics are still observable, indicating the device's capability of acting as a wearable or even implantable artificial synapse. Yet when the device is bent from r = 8 mm to 5 mm, the overall device current and synaptic potentiation/depression characteristics gradually vanish. The optical microscope image reveals that this phenomenon might be related with the formation of cracks throughout the thin film which can increase the resistance of the device (Fig. S9, ESI†). Not only does the bending radius have some influence on the synaptic potentiation and synaptic depression characteristics, but also the number bending cycles. When the bending radius is equal to 16 mm (r = 16 mm), the synaptic potentiation and synaptic depression characteristics vanish gradually over 100 bending cycles (Fig. S10, ESI†).

Conclusions

To summarize, an organic material based artificial synapse is fabricated directly on a flexible PET substrate, exhibiting distinctive history-dependent memristive behaviour that is similar to synaptic potentiation and depression in neurobiology.

Essential synaptic plasticity and some memory and learning behaviours of human beings have been demonstrated, suggesting that our device is promising to meet the basic demands for constructing neuromorphic information storage and processing systems. More importantly, the device still exhibits synaptic potentiation and depression characteristics when bent 100 times with a bending radius of less than 10 mm. The findings demonstrate that the work, including the measurement of synaptic performance in the bent state and the influence of bending radius and number of bending cycles on synaptic simulation, is favourable for the development of wearable neuromorphic computing systems.

Acknowledgements

This work was supported by the State Key Project of Fundamental Research of China (973 Program, 2012CB933004), National Natural Science Foundation of China (51303194, 61328402, 61306152, 11474295, 61574146 and 51525103), the Instrument Developing Project of the Chinese Academy of Sciences (YZ201327), the Youth Innovation Promotion Association of the Chinese Academy of Sciences, Ningbo Major Project for Science and Technology (2014B11011), Ningbo Science and Technology Innovation Team (2015B11001), Ningbo Natural Science Foundation (2014A610152), Ningbo International Cooperation Projects (2014D10005) and National Science Council (NSC) of Taiwan (NSC100-2221-E-027-024-MY3).

Notes and references

1 V. M. Ho, J.-A. Lee and K. C. Martin, *Science*, 2011, **334**, 623.
2 G. Perea, M. Nevarrete and A. Araque, *Trends Neurosci.*, 2009, **32**, 421.
3 D. Drachman, *Neurology*, 2005, **64**, 2004.
4 C. Koch and I. Segev, *Nat. Neurosci.*, 2000, **3**, 1171.
5 D. Choquet and A. Triller, *Neuron*, 2013, **80**, 691.
6 L. F. Abbott and S. B. Nelson, *Nat. Neurosci.*, 2000, **3**, 1178.
7 G. Q. Bi and M. M. Poo, *J. Neurosci.*, 1998, **18**, 10464.
8 Q. Lai, L. Zhang, Z. Li, W. F. Stickle, R. S. Williams and Y. Chen, *Adv. Mater.*, 2010, **22**, 2448.
9 K. Seo, I. Kim, S. Jung, M. Jo, S. Park, J. Park, J. Shin, K. P. Biju, J. Kong, K. Lee, B. Lee and H. Hwang, *Nanotechnology*, 2011, **22**, 254023.
10 T. Chang, S. H. Jo and W. Lu, *ACS Nano*, 2011, **5**, 7669.
11 B. Pakkenberg, D. Pelvig, L. Marner, M. J. Bundgaard, H. J. G. Gundersen, J. R. Nyengaard and L. Regeur, *Exp. Gerontol.*, 2003, **38**, 95.
12 B. Pakkenberg and H. J. G. Gundersen, *J. Comp. Neurol.*, 1997, **384**, 312.
13 G. Indiveri, E. Chicca and R. Douglas, *IEEE Trans. Neur. Networ.*, 2006, **17**, 211.
14 G. Rachmuth and C. S. Poon, *HFSP J.*, 2008, **2**, 156.
15 Y. H. Liu, L. Q. Zhu, P. Feng, Y. Shi and Q. Wan, *Adv. Mater.*, 2015, **27**, 37.
16 J. B. Lont and W. Guggenbuhl, *IEEE Trans. Neur. Networ.*, 1992, **3**, 457.
17 D. Kuzum, R. G. D. Jeyasingh, B. Lee and H. S. P. Wong, *Nano Lett.*, 2012, **12**, 2179.
18 F. Pan, S. Gao, C. Chen, C. Song and F. Zeng, *Mater. Sci. Eng., R*, 2014, **83**, 1.
19 T. Ohno, T. Hasegawa, T. Tsuruoka, K. Terabe, J. Gimzewski and M. Aono, *Nat. Mater.*, 2011, **10**, 591.
20 Z. Q. Wang, H. Y. Xu, X. H. Li, H. Yu, Y. C. Liu and X. J. Zhu, *Adv. Funct. Mater.*, 2012, **22**, 2759.
21 T. Chang, S. H. Jo, K. H. Kim, P. Sheridan, S. Gaba and W. Lu, *Appl. Phys. A: Mater. Sci. Process.*, 2011, **102**, 857.
22 S. Z. Li, F. Zeng, C. Chen, H. Y. Liu, G. S. Tang, S. Gao, C. Song, Y. S. Lin, F. Pan and D. Guo, *J. Mater. Chem. C*, 2013, **1**, 5292.
23 W. He, K. J. Huang, N. Ning, K. Ramanathan, G. Q. Li, Y. Jiang, J. Y. Sze, L. P. Shi, R. Zhao and J. Pei, *Sci. Rep.*, 2014, **4**, 4755.
24 E. E. Josberger, Y. X. Deng, W. Sun, R. Kautz and M. Rolandi, *Adv. Mater.*, 2014, **26**, 4986.
25 T. Chang, S.-H. Jo and W. Lu, *ACS Nano*, 2011, **5**, 7669.
26 M. K. Hota, M. K. Bera, B. Kundu, S. C. Kundu and C. K. Maiti, *Adv. Funct. Mater.*, 2012, **22**, 4493.
27 Y. Li, Y. P. Zhong, J. J. Zhang, L. Xu, Q. Wang, H. J. Sun, H. Tong, X. M. Cheng and X. S. Miao, *Sci. Rep.*, 2014, **4**, 4906.
28 C. Du, W. Ma, T. Chang, P. Sheridan and W. D. Lu, *Adv. Funct. Mater.*, 2015, **25**, 4290.
29 B. L. Hu, X. J. Zhu, X. X. Chen, L. Pan, S. S. Peng, Y. Z. Wu, J. Shang, G. Liu, Q. Yan and R.-W. Li, *J. Am. Chem. Soc.*, 2012, **134**, 17408.
30 C. L. Liu and W. C. Chen, *Polym. Chem.*, 2011, **2**, 2169.
31 D. M. Sun, Z. M. Yang, Z. J. Ren, H. H. Li, M. R. Bryce, D. G. Ma and S. K. Yan, *Chem. – Eur. J.*, 2014, **20**, 16233.
32 F. Zeng, S. Z. Li, J. Yang, F. Pan and D. Guo, *RSC Adv.*, 2014, **4**, 14822.
33 C. Wang, G. Liu, Y. Chen, R.-W. Li, W. B. Zhang, L. X. Wang and B. Zhang, *J. Mater. Chem. C*, 2015, **3**, 664.
34 G. Liu, C. Wang, W. B. Zhang, L. Pan, C. C. Zhang, X. Yang, F. Fan, Y. Chen and R.-W. Li, *Adv. Electron. Mater.*, 2015, 1500298.
35 G. D. Wu, J. Zhang, X. Wan, Y. Yang and S. H. Jiang, *J. Mater. Chem. C*, 2014, **2**, 6249.
36 N. Gergel-Hackett, J. L. Tedesco and C. A. Richter, *Proc. IEEE*, 2012, **100**, 1971.
37 Y. Shirota, *J. Mater. Chem.*, 2000, **10**, 1.
38 Y. Song, C. Di, X. Yang, S. Li, W. Xu, Y. Liu, L. Yang, Z. Shuai, D. Zhang and D. Zhu, *J. Am. Chem. Soc.*, 2006, **128**, 15940.
39 R. Kumar, R. G. Pillai, N. Pekas, Y. L. Wu and R. L. McCreery, *J. Am. Chem. Soc.*, 2012, **134**, 14869.
40 B. C. Das, R. G. Pillai, Y. L. Wu and R. L. McCreery, *ACS Appl. Mater. Interfaces*, 2013, **5**, 11052.
41 B. Han, Z. Li, T. Wandlowski, A. Błaszczyk and M. Mayor, *J. Phys. Chem. C*, 2007, **111**, 13855.
42 B. Sun, P. Tehrani, N. D. Robinson and D. Brandell, *J. Mater. Sci.*, 2013, **48**, 5756.

43 S. H. Hsiao, H. M. Wang, P. C. Chang, Y. R. Kung and T. M. Lee, *J. Polym. Sci., Part A: Polym. Chem.*, 2013, **51**, 2925.
44 D. J. Liaw, K. L. Wang, Y. C. Huang, K. R. Lee, J. Y. Lai and C. S. Ha, *Prog. Polym. Sci.*, 2012, **37**, 907.
45 R. C. Aktinson and R. M. Shiffrin, *The Psychology of Learning and Motivation: Advances in Research and Theory*, Academic Press, New Work, 1968, p. 89.
46 M. E. Bear, B. W. Connors and M. A. Paradiso, *Neuroscience: Exploring the Brain*, High Education Press, Beijing, 2007, p. 761, ISBN 078-1-7600-38.
47 P. D. Grimwood, S. J. Martin and R. G. M. Morris, *Synapse*, John Hopkins University Press, Baltimore, 2001, p. 519.
48 A. K. Vogt, G. Wrobel, W. Meyer, W. Knoll and A. Offenhausser, *Biomaterials*, 2005, **26**, 2549.
49 S. J. Martin, P. D. Grimwood and R. G. M. Morris, *Annu. Rev. Neurosci.*, 2000, **23**, 649.
50 R. S. Zucker, *Curr. Opin. Neurobiol.*, 1999, **9**, 305.
51 A. M. Zador and L. E. Dobrunz, *Neuron*, 1997, **19**, 1.
52 R. S. Zucker, *Annu. Rev. Neurosci.*, 1989, **12**, 13.
53 T. Sippy, A. Cruz-Martin, A. Jeromin and F. E. Schweizer, *Nat. Neurosci.*, 2003, **6**, 1031.
54 F. Doussau, A. Clabecq, J. P. Henry, F. Darchen and B. Poulain, *J. Neurosci.*, 1998, **18**, 3147.
55 R. S. Zucker and W. G. Regehr, *Annu. Rev. Physiol.*, 2002, **64**, 355.
56 D. Gardner and C. Stevens, *J. Physiol.*, 1980, **304**, 145.
57 T. V. Bliss and T. Lomo, *J. Physiol.*, 1973, **232**, 331.
58 A. U. Larkman and J. J. Jack, *Curr. Opin. Neurobiol.*, 1995, **5**, 324.
59 S. M. Dudek and M. F. Bear, *Proc. Natl. Acad. Sci. U. S. A.*, 1992, **89**, 4363.
60 G. J. Rose and E. S. Fortune, *J. Neurosci.*, 1999, **19**, 7629.
61 E. S. Fortune and G. J. Rose, *J. Neurosci.*, 2000, **20**, 7122.
62 G. Q. Bi and M. M. Poo, *Annu. Rev. Neurosci.*, 2001, **24**, 139.
63 Y. Dan and M. M. Poo, *Physiol. Rev.*, 2006, **86**, 1033.
64 J. L. McGaugh, *Science*, 2000, **287**, 248.
65 P. P. Atluri and W. G. Regehr, *J. Neurosci.*, 1996, **16**, 5661.
66 G. Daoudal and D. Debanne, *Learn. Mem.*, 2003, **10**, 456.
67 J. A. Kauer and R. C. Malenka, *Nat. Rev. Neurosci.*, 2007, **8**, 844.
68 C. H. Bailey and E. R. Kandel, *Annu. Rev. Physiol.*, 1993, **55**, 397.
69 R. M. Shiffrin and R. C. Atkinson, *Psychol. Rev.*, 1969, **76**, 179.
70 G. G. Turrigiano, K. R. Leslie, N. S. Desai, L. C. Rutherford and S. B. Nelson, *Nature*, 1998, **391**, 892.
71 M. Makhinson, J. K. Chotiner, J. B. Watson and T. J. O'Dell, *J. Neurosci.*, 1999, **19**, 2500.
72 F. I. Craik and M. J. Watkins, *J. Verb. Learning Verb. Behav.*, 1973, **12**, 599.
73 M. J. Anzanello and F. S. Fogliatto, *Int. J. Ind. Ergonom.*, 2011, **41**, 573.
74 S. G. Hu, Y. Liu, T. P. Chen, Z. Liu, Q. Yu, L. J. Deng, Y. Yin and S. Hosaka, *Appl. Phys. Lett.*, 2013, **103**, 133701.